746 *Chem. Mater.* **2010,** *22,* 746–754
DOI:10.1021/cm9012014

CHEMISTRY OF MATERIALS
Article

Synthesis, Characterization, and Lithium Storage Capability of $AMoO_4$ (A = Ni, Co) Nanorods†

Wei Xiao, Jun Song Chen, Chang Ming Li, Rong Xu, and Xiong Wen Lou*

School of Chemical and Biomedical Engineering, Nanyang Technological University, 70 Nanyang Drive, Singapore 637457, Singapore

Received April 30, 2009. Revised Manuscript Received July 6, 2009

One-dimensional (1D) $AMoO_4 \cdot nH_2O$ (A = Ni, Co) nanorods have been synthesized by a facile hydrothermal method. The effect of different synthetic conditions on the morphologies of the final products was systematically investigated. The size of the nanorods can be easily controlled by adding ethanol in the synthetic solution. For the first time, the self-assembled growth of oriented $NiMoO_4 \cdot nH_2O$ nanorod arrays on Ti-foil substrates was achieved. The thermal dehydration and phase transformation processes of $AMoO_4 \cdot nH_2O$ nanorods were thoroughly investigated by TG-DTA and time-resolved synchrotron XRD. As-prepared hydrate nanorods can be further converted to corresponding $AMoO_4$ nanorods by annealing at 300−600 °C for 1 h without significant alteration of 1D morphology. Electrochemical lithium storage capabilities of dehydrated $AMoO_4$ nanorods have been investigated. The results suggest their potential use as cathode materials for lithium ion batteries.

1. Introduction

In the past decade, synthesis of one-dimensional (1D) materials has attracted much research interest due to their unique properties and applications.[1−5] To date, 1D nanostructures (nanorods, nanowires, nanoribbons, nanotubes, etc.) have been synthesized for many important materials such as semiconductor, metal and metal oxide, sulfide, and so forth by employing various synthetic approaches. These mainly include template method,[6−8] vapor−liquid−solid method,[5] and wet chemical routes.[9,10] Among them, wet chemical routes such as hydrothermal or solvothermal synthesis have emerged as an efficient and cheap method for preparation of low dimensional nanomaterials.[10−12] Nanostructured materials lie in the center of fundamental advances to high-efficiency electrochemical energy storage/conversion devices, such as lithium-ion batteries (LIBs).[13−21] In particular, oriented 1D nanomaterials are acknowledged as one of the promising solutions to future generation of lithium ion batteries with high energy density, high power density, and excellent cycling stability, because of their large surface area, short distance for mass and charge transport, and freedom for volume change.[13−16]

Metal molybdates and tungstates stand as two important families of inorganic materials which have been a subject of intensive research due to their many applications such as photoluminescence,[22−24] magnetic properties,[25−28] electronic

† Accepted as part of the 2010 "Materials Chemistry of Energy Conversion Special Issue".

*Corresponding author. E-mail: xwlou@ntu.edu.sg. Tel: +65-63168879. Fax: +65-67911761.

(1) Kolmakov, A.; Moskovits, M. *Ann. Rev. Mater. Res.* **2004**, *34*, 151.
(2) Rao, C. N. R.; Deepak, F. L.; Gundiah, G.; Govindaraj, A. *Prog. Solid State Chem.* **2003**, *31*, 5.
(3) Xia, Y. N.; Yang, P. D.; Sun, Y. G.; Wu, Y. Y.; Mayers, B.; Gates, B.; Yin, Y. D.; Kim, F.; Yan, Y. Q. *Adv. Mater.* **2003**, *15*, 353.
(4) Tang, Z. Y.; Kotov, N. A. *Adv. Mater.* **2005**, *17*, 951.
(5) Law, M.; Goldberger, J.; Yang, P. D. *Ann. Rev. Mater. Res.* **2004**, *34*, 83.
(6) Hurst, S. J.; Payne, E. K.; Qin, L. D.; Mirkin, C. A. *Angew. Chem., Int. Ed.* **2006**, *45*, 2672.
(7) Cheng, F. Y.; Tao, Z. L.; Liang, J.; Chen, J. *Chem. Mater.* **2008**, *20*, 667.
(8) Bae, C.; Yoo, H.; Kim, S.; Lee, K.; Kim, J.; Sung, M. M.; Shin, H. *Chem. Mater.* **2008**, *20*, 756.
(9) Choy, J. H.; Jang, E. S.; Won, J. H.; Chung, J. H.; Jang, D. J.; Kim, Y. W. *Adv. Mater.* **2003**, *15*, 1911.
(10) Tang, K. B.; Qian, Y. T.; Zeng, J. H.; Yang, X. G. *Adv. Mater.* **2003**, *15*, 448.
(11) Liu, B.; Zeng, H. C. *J. Am. Chem. Soc.* **2003**, *125*, 4430.
(12) Wang, X.; Li, Y. D. *J. Am. Chem. Soc.* **2002**, *124*, 2880.
(13) Liu, J.; Cao, G. Z.; Yang, Z. G.; Wang, D. H.; Dubois, D.; Zhou, X. D.; Graff, G. L.; Pederson, L. R.; Zhang, J. G. *ChemSusChem* **2008**, *1*, 676.
(14) Bruce, P. G.; Scrosati, B.; Tarascon, J. M. *Angew. Chem., Int. Ed.* **2008**, *47*, 2930.
(15) Wang, Y.; Cao, G. Z. *Adv. Mater.* **2008**, *20*, 2251.
(16) Guo, Y. G.; Hu, J. S.; Wan, L. J. *Adv. Mater.* **2008**, *20*, 2878.
(17) Simon, P.; Gogotsi, Y. *Nat. Mater.* **2008**, *7*, 845.
(18) Lou, X. W.; Deng, D.; Lee, J. Y.; Archer, L. A. *J. Mater. Chem.* **2008**, *18*, 4397.
(19) Lou, X. W.; Deng, D.; Lee, J. Y.; Archer, L. A. *Chem. Mater.* **2008**, *20*, 6562.
(20) Lou, X. W.; Deng, D.; Lee, J. Y.; Feng, J.; Archer, L. A. *Adv. Mater.* **2008**, *20*, 258.
(21) Lou, X. W.; Archer, L. A.; Yang, Z. C. *Adv. Mater.* **2008**, *20*, 3987.
(22) Liu, B.; Yu, S. H.; Li, L. J.; Zhang, Q.; Zhang, F.; Jiang, K. *Angew. Chem., Int. Ed.* **2004**, *43*, 4745.
(23) Luo, Y. S.; Zhang, W. D.; Dai, X. J.; Yang, Y.; Fu, S. Y. *J. Phys. Chem. B* **2009**, *113*, 4856.
(24) Liu, J. P.; Huang, X. T.; Li, Y. Y.; Li, Z. K. *J. Mater. Chem.* **2007**, *17*, 2754.
(25) Vilminot, S.; Andre, G.; Kurmoo, M. *Inorg. Chem.* **2009**, *48*, 2687.
(26) Chu, W. G.; Wang, H. F.; Guo, Y. J.; Zhang, L. N.; Han, Z. H.; Li, Q. Q.; Fan, S. S. *Inorg. Chem.* **2009**, *48*, 1243.
(27) Zhang, F.; Yiu, Y.; Aronson, M. C.; Wong, S. S. *J. Phys. Chem. C* **2008**, *112*, 14816.
(28) Ding, Y.; Wan, Y.; Min, Y. L.; Zhang, W.; Yu, S. H. *Inorg. Chem.* **2008**, *47*, 7813.
(29) Rodriguez, J. A.; Chaturvedi, S.; Hanson, J. C.; Albornoz, A.; Brito, J. L. *J. Phys. Chem. B* **1998**, *102*, 1347.

 Published on Web 08/05/2009

properties,[29,30] and catalysis.[26,28,31−35] For example, cobalt and nickel molybdates are important components of industrial catalysts for the partial oxidation of hydrocarbons and precursors in the synthesis of sulfide, nitride, and carbide materials.[36−39] In general, these molybdates can be seen as the product of adding CoO or NiO to MoO_3. There are three basic types of $AMoO_4$ (A = Co, Ni) existing under atmospheric pressure, namely, the low temperature α-$AMoO_4$, the high temperature β-$AMoO_4$, and the hydrate $AMoO_4 \cdot nH_2O$,[29,33] while another one, $AMoO_4$-II, is observed at higher pressures.[40] The most compelling structural difference between α and β phases is in the coordination of the Mo^{6+} ions, being octahedral and tetrahedral in the α and β phase respectively.[29,33] Although the structures of hydrated $AMoO_4 \cdot nH_2O$ compounds are less known, they may be used as advantageous precursors for fabrication of other structures and various catalysts due to their relatively low decomposition temperature (200−400 °C) .[33,36]

1D nanostuctures of molybdates and tungstates are expected to have novel properties induced by their reduced dimensionality. Although 1D nanomaterials of various tungstates such as Ag−W−O,[31] Bi_2WO_6,[31] $ZnWO_4$,[31] $MnWO_4$,[31,41] $FeWO_4$,[31] $CdWO_4$,[42,43] and $BaWO_4$[44,45] have been successfully synthesized, to the best of our knowledge, there are only few reports for synthesis of nanorods or nanowires of molybdates.[26,28,32,46,47] This may be due to the fact that, unlike tungstates, molybdates will easily form hydrates which make it difficult to synthesize molybdates by the wet-chemical route.[48−50] And the above-mentioned synthetic routes require somewhat complex precursors or high temperature treatments or prudent pH selections, which definitely restrict the large-scale productions and potential applications of the nano-molybdates. In addition, the lithium storage capabilities of molybdates have received little attention by far;[28,51−53] most works have focused on their possible applications as anode materials, and their possible applications as cathode materials still remain largely unexplored.[54,55] The wide variety in composition and structure of these molybdates might make tuning the lithium storage capabilities of molybdates possible. We have previously synthesized α-MoO_3 nanorods and $W_{18}O_{49}$ nanowires employing hydrothermal methods without using any organic surfactant.[56−58] These 1D crystal growths are largely induced by the intrinsic structural anisotropy. In this work, we report the facile synthesis of $AMoO_4 \cdot nH_2O$ (A = Ni, Co) nanorods through a hydrothermal route and their size control and direct self-assembly of the oriented nanorods on Ti-foil substrates. The dehydration processes have also been thoroughly investigated. The initial morphology of these hydrate precursors can be retained after calcination. This approach may serve as a plausible alternative for synthesis of 1D nanomaterials.[50] Furthermore, the lithium storage capability of $AMoO_4$ (A = Ni, Co) nanorods has been investigated and the feasibility of $AMoO_4$ (A = Ni, Co) nanorods as cathode materials for LIBs has been clearly demonstrated.

2. Experimental Section

2.1. Materials Preparation. All chemicals were purchased from Aldrich and used as received without further purification. $AMoO_4 \cdot nH_2O$ nanorods were synthesized employing a simple hydrothermal recrystallization method with or without adding ethanol as a cosolvent. For a typical synthesis, an aqueous solution of either $Ni(NO_3)_2$ or $Co(NO_3)_2$ was added to an equal volume of Na_2MoO_4 solution (0.1 M for all solutions unless otherwise stated) under constant magnetic stirring. To this solution, a specific amount of pure ethanol was added in to achieve a volumetric ratio (r) of ethanol/water in the range of 0−2. There was no precipitate formed until a certain amount of ethanol was added in. However, there will be instantaneous light purple (H_2O−$CoMoO_4$) or yellow (H_2O−$NiMoO_4$) precipitate when solutions of 0.4 M are used. To obtain vertically aligned nanorods on Ti-foil substrates, a 0.1 mm × 10 mm × 60 mm Ti foil was placed in the autoclaves before heating. The resulting mixture was then autoclaved in an electric oven at 140−200 °C for a period of 2−24 h. After heating, the autoclave was cooled down to room temperature using tap water. The solid product was harvested by centrifugation and washed with deionized water three times and acetone once before room temperature vacuum drying. As-prepared hydrate precursors were postannealed

(30) Rodriguez, J. A.; Hanson, J. C.; Chaturvedi, S.; Maiti, A.; Brito, J. L. *J. Phys. Chem. B* **2000**, *104*, 8145.
(31) Yu, S. H.; Liu, B.; Mo, M. S.; Huang, J. H.; Liu, X. M.; Qian, Y. T. *Adv. Funct. Mater.* **2003**, *13*, 639.
(32) Cui, X. J.; Yu, S. H.; Li, L. L.; Biao, L.; Li, H. B.; Mo, M. S.; Liu, X. M. *Chem.—Eur. J.* **2004**, *10*, 218.
(33) Rodriguez, J. A.; Chaturvedi, S.; Hanson, J. C.; Brito, J. L. *J. Phys. Chem. B* **1999**, *103*, 770.
(34) Ma, D.; Huang, S.; Chen, W.; Hu, S.; Shi, F.; Fan, K. *J. Phys. Chem. C* **2009**, *113*, 4369.
(35) Zhang, L. W.; Wang, Y. J.; Cheng, H. Y.; Yao, W. Q.; Zhu, Y. F. *Adv. Mater.* **2009**, *21*, 1286.
(36) Brito, J. L.; Barbosa, A. L. *J. Catal.* **1997**, *171*, 467.
(37) Liang, C. H.; Ma, W. P.; Feng, Z. C.; Li, C. *Carbon* **2003**, *41*, 1833.
(38) Hada, K.; Nagai, M.; Omi, S. *J. Phys. Chem. B* **2001**, *105*, 4084.
(39) Jaksic, J. M.; Vojnovic, M. V.; Krstajic, N. V. *Electrochim. Acta* **2000**, *45*, 4151.
(40) Livage, C.; Hynaux, A.; Marrot, J.; Nogues, M.; Ferey, G. *J. Mater. Chem.* **2002**, *12*, 1423.
(41) Chen, S. J.; Chen, X. T.; Xue, Z.; Zhou, J. H.; Li, J.; Hong, J. M.; You, X. Z. *J. Mater. Chem.* **2003**, *13*, 1132.
(42) Yu, S. H.; Antonietti, M.; Colfen, H.; Giersig, M. *Angew. Chem., Int. Ed.* **2002**, *41*, 2356.
(43) Liao, H. W.; Wang, Y. F.; Liu, X. M.; Li, Y. D.; Qian, Y. T. *Chem. Mater.* **2000**, *12*, 2819.
(44) Shi, H. T.; Qi, L. M.; Ma, J. M.; Cheng, H. M. *J. Am. Chem. Soc.* **2003**, *125*, 3450.
(45) Kwan, S.; Kim, F.; Akana, J.; Yang, P. D. *Chem. Commun.* **2001**, 447.
(46) Peng, C.; Gao, L.; Yang, S. W.; Sun, J. *Chem. Commun.* **2008**, 5601.
(47) Wang, L.; Peng, B.; Guo, X. F.; Ding, W. P.; Chen, Y. *Chem. Commun.* **2009**, 1565.
(48) Hangloo, V.; Pandita, S.; Bamzai, K. K.; Kotru, P. N.; Sahni, N. *Cryst. Growth Design* **2003**, *3*, 753.
(49) Barnes, N.; Kitchin, S. J.; Hriljac, J. A. *Inorg. Chem.* **1999**, *38*, 6317.
(50) Niederberger, M.; Krumeich, F.; Muhr, H. J.; Muller, M.; Nesper, R. *J. Mater. Chem.* **2001**, *11*, 1941.
(51) Sharma, N.; Shaju, K. M.; Subba Rao, G. V.; Chowdari, B. V. R.; Dong, Z. L.; White, T. J. *Chem. Mater.* **2004**, *16*, 504.
(52) Leyzerovich, N. N.; Bramnik, K. G.; Buhrmester, T.; Ehrenberg, H.; Fuess, H. *J. Power Sources* **2004**, *127*, 76.
(53) Kim, S. S.; Ogura, S.; Ikuta, H.; Uchimoto, Y.; Wakihara, M. *Solid State Ionics.* **2002**, *146*, 249.
(54) Pietro, B. D.; Scrosati, B.; Bonino, F.; Lazzari, M. *J. Electrochem. Soc.* **1979**, *126*, 729.
(55) Bonino, F.; Lazzari, M.; Scrosati, B. *J. Electrochem. Soc.* **1984**, *131*, 610.
(56) Lou, X. W.; Zeng, H. C. *Chem. Mater.* **2002**, *14*, 4781.
(57) Lou, X. W.; Zeng, H. C. *J. Am. Chem. Soc.* **2003**, *125*, 2697.
(58) Lou, X. W.; Zeng, H. C. *Inorg. Chem.* **2003**, *42*, 6169.

at various temperatures for 1 h to obtain the $AMoO_4$ (A = Ni, Co) with the heating rate of 5 °C min^{-1}.

2.2. Materials Characterization. Crystallographic information of all as-prepared samples was investigated with X-ray powder diffraction (XRD; Shimadzu XRD-6000, Cu Kα, λ = 1.5406 Å) at a scanning rate of 1 °C min^{-1}. Thermal behavior of samples was analyzed by simultaneous thermogravimetry (TG) and differential thermal analysis (DTA) (Shimadzu DTG-60). The samples were heated from room temperature up to 600 °C at a heating rate of 5 °C min^{-1} in a dynamic atmosphere of air (35 mL min^{-1}) using α-alumina crucibles. The bonding properties of the hydrate precursors and products after calcination were characterized with Fourier transform infrared spectroscopy (FTIR, Shimadzu FTIR-8700) using a standard potassium bromide (KBr) pellet technique. Each FTIR spectrum was collected after 32 scans at a resolution of 2 cm^{-1} from 400 to 4000 cm^{-1}. The morphology of as-prepared samples was examined before and after annealing with field-emission scanning electron microscopy (FESEM; JSM-6700F, with EDX) and high-resolution analytical transmission electron microscopy (TEM/HRTEM, JEM-2010, 200 kV, with ED; HRTEM, Philips FEG CM300, 300 kV; and FETEM, JEM-2010F, with ED and FFT). Selected area electron diffraction (SAED) was used to examine the samples' crystallinities. Elemental compositions of prepared samples were measured with energy dispersive spectroscopy (EDX) microanalysis attached to FESEM.

2.3. Electrochemical Characterization. The electrochemical measurements on lithium storage capability were carried out using homemade two-electrode Swagelok-type cells with lithium metal as the counter and reference electrodes at room temperature. The working electrode consisted of 80 wt % of the active material (e.g., $AMoO_4$ nanorods), 10 wt % of conductivity agent (carbon black, Super-P-Li), and 10 wt % of binder (polyvinylidene difluoride, PVDF, Aldrich). The electrolyte was 1 M $LiPF_6$ in a 50:50 (w/w) mixture of ethylene carbonate and diethyl carbonate. Cell assembly was carried out in an Ar-filled glovebox with the concentrations of moisture and oxygen below 1 ppm. Cyclic voltammetry (CV, 0.5 mV s^{-1}) and galvanostatic charge/discharge cycling (50 mA g^{-1}) were carried out with an electrochemical workstation (CHI 660C) and a battery tester (NEWARE), respectively.

3. Results and Discussion

Figure 1A displays two typical XRD patterns of as-prepared $NiMoO_4 \cdot nH_2O$ products. As can be seen, the XRD patterns of as-prepared $NiMoO_4 \cdot nH_2O$ hydrate with or without ethanol are very similar except that a slight difference is observed for the peaks between 10 and 15°. Both patterns agree well with the reported pattern for nickel molybdate hydrate (JCPDS card no. 13-0128).[29,33] Figure 1B shows the XRD patterns of $CoMoO_4 \cdot nH_2O$ samples prepared with or without addition of ethanol. In general, they are similar to reported patterns (JCPDS card no. 26-0477) indicating the same form of basic structure for these hydrate compounds.[29,33,36] For synthesis of $CoMoO_4 \cdot nH_2O$, the crystal phases of resulting products are strongly dependent on the synthetic conditions. It was reported that a similar hydrothermal synthesis at 200 °C with addition of other organic additives produces the high pressure phase $CoMoO_4$-II, and lowering the reaction temperature leads to $CoMoO_4 \cdot nH_2O$ phase.[40] In our synthesis, some slight variations are

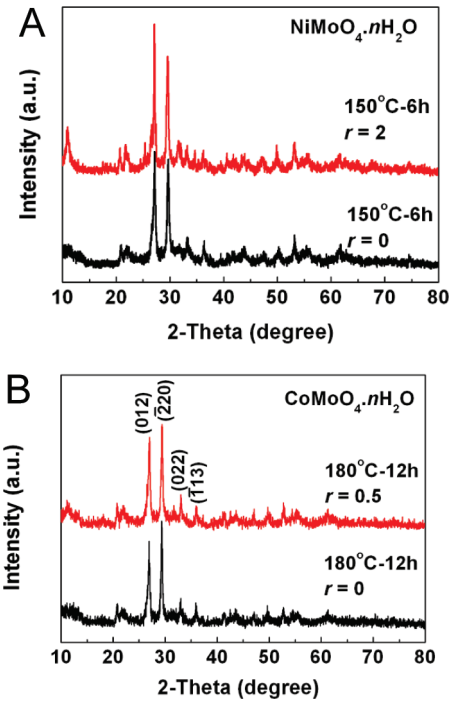

Figure 1. Representative XRD patterns of $NiMoO_4 \cdot nH_2O$ (A) and $CoMoO_4 \cdot nH_2O$ (B) products prepared with or without adding ethanol as indicated by the *r* values.

observed from the XRD patterns (Figure 1B) due to change of reaction temperature and addition of ethanol. These minor differences could be attributed to different extents of hydration as will be confirmed by TGA and FTIR analysis below. To investigate whether organic species are adsorbed onto the solid samples, FTIR spectra of representative samples are collected as shown in Figure 2. It is evident that the spectra (Figure 2A, a and b; Figure 2B, a and b) of the samples prepared with or without adding ethanol are essentially identical, and they agree well with reported spectra in literature.[36] This observation further confirms the formation of $AMoO_4 \cdot nH_2O$ phases. The elemental compositions of as-prepared nanorods are confirmed by EDX (not shown). We examined many samples and found that the Ni/Mo and Co/Mo ratios are generally in the range of 0.9−1.1, which should be considered consistent with the stoichiometric value of 1 within the technique's intrinsic accuracy.

Figure 3 displays our $NiMoO_4 \cdot nH_2O$ nanorods synthesized with or without adding ethanol as a cosolvent. As shown in Figure 3A, long nanorods up to 10 μm with diameters in the range of 50−100 nm are synthesized without adding ethanol. As obvious from the images, the nanorods aggregate to form bundles which are also observed for $MoO_3 \cdot H_2O$ nanofibers.[50] Experiments are conducted in the temperature range of 140−200 °C. It was found that syntheses at 140 °C produce a large amount of microparticles in the shape of flowers and spheres (not shown here) in addition to nanorods, while only short nanorods (up to a few micrometers) are produced at 180 °C. Therefore, 150 °C is generalized as an appropriate temperature for synthesis of $NiMoO_4 \cdot nH_2O$ nanorods. It

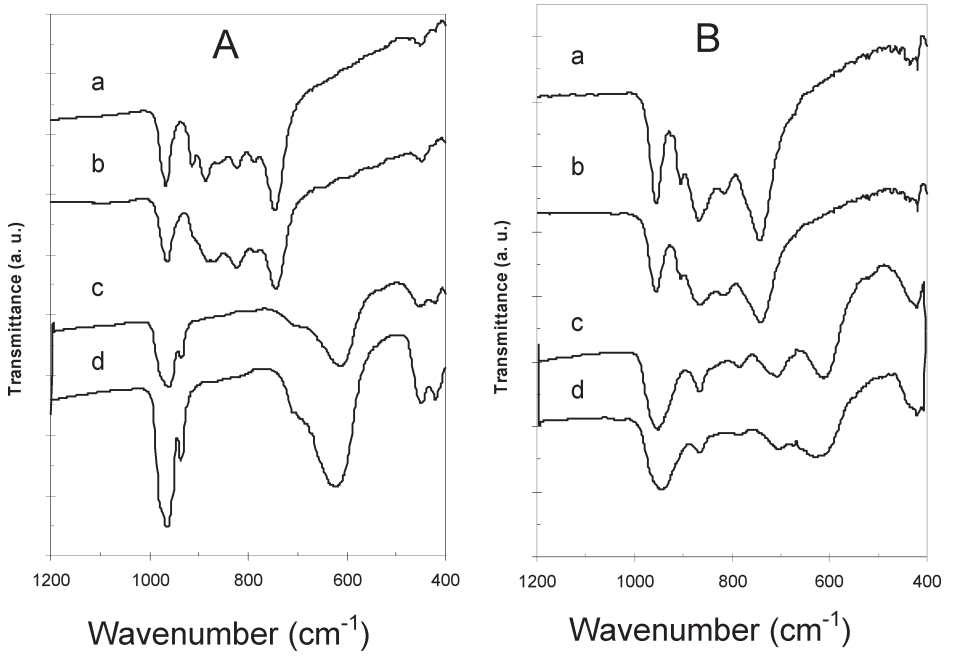

Figure 2. (A) FTIR spectra of Ni−Mo samples: (a) prepared at 150 °C for 6 h with $r = 0$; (b) similar to (a) but with $r = 2$; (c) and (d) samples obtained by calcining (a) and (b) at 450 °C for 1 h, respectively. (B) Co−Mo samples: (a) hydrate samples prepared at 180 °C for 12 h with $r = 0$; (b) similar to (a) but with $r = 0.5$; (c) and (d) samples obtained by calcining (a) and (b) at 350 °C for 1 h, respectively.

is well-known that adding organic additives during synthesis of inorganic materials will drastically change the morphology and microstructure of the resulting inorganic materials. In the present study, the size control is achieved by adding ethanol to the synthesis solution. Figure 3B displays the nearly monodispersed $NiMoO_4 \cdot nH_2O$ nanorods synthesized by addition of 2 times of ethanol ($r = 2$) into the synthesis solution. These nanorods are much shorter (generally less than 1 μm) with diameters in the range of 20−30 nm. In fact, these smaller nanorods are needle-like on both ends with a nonuniform diameter along the whole length, which is evident from Figure 3B. Again, the individual nanorods easily form bundles (Figure 3B) largely through interactions of their highly unsaturated sidewalls.[58] When the synthesis temperature is increased to 180 °C, it is found that some microplatelets (Figure 3D) made of primary particles coexist with nanorods. Such microplatelets constitute a significant part of the as-prepared material at 200 °C.

We also studied for the first time the self-assembled growth of $NiMoO_4 \cdot nH_2O$ nanorod array on Ti-foil substrates. Figure 3E,F shows the SEM and optical images of the self-assembled $NiMoO_4 \cdot nH_2O$ nanorods on Ti-foil substrates. The optical image (Figure 3E, inset) shows that a uniform yellow film has grown on the Ti-foil. The top-view SEM images depict that the uniform self-assembled film consists of aligned nanowire arrays growing directly on the Ti-foil. It is well acknowledged that such self-supported nanowire arrays grown directly on a conducting substrate represent an attractive architecture for many applications such as batteries, supercapacitors, sensors, catalysts, solar cells, and so on.[13,59−61] Aligned $NiMoO_4 \cdot nH_2O$ nanorod arrays have also been successfully

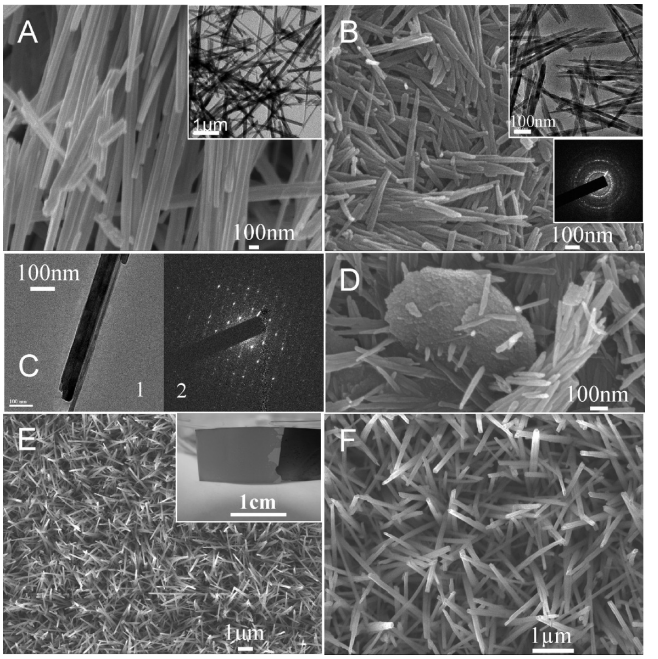

Figure 3. (A) FESEM image and TEM image (inset) of $NiMoO_4 \cdot nH_2O$ sample (150 °C, 6 h, $r = 0$); (B) FESEM image, TEM image, and SAED (inset) of $NiMoO_4 \cdot nH_2O$ sample (150 °C, 6 h, $r = 2$). The inset is a SAED pattern taken based on many nanorods; (C) 1 is high magnification TEM image of (a), and 2 is a SAED pattern taken based on one individual nanorod; (D) FESEM image of sample (180 or 200 °C, 6 h, $r = 2$); (E) and (F) FESEM image showing top view of nearly vertically oriented $NiMoO_4 \cdot nH_2O$ nanorod arrays directly grown on Ti foil (150 °C, 6 h, $r = 0$); inset is an optical image of the self-assembled $NiMoO_4 \cdot nH_2O$ film on Ti foil.

(59) Li, Y. G.; Tan, B.; Wu, Y. Y. *Nano Lett.* **2008**, *8*, 265.
(60) Liu, J. P.; Li, Y. Y.; Ding, R.; Jiang, J.; Hu, Y. Y.; Ji, X. X.; Chi, Q. B.; Zhu, Z. H.; Huang, X. T. *J. Phys. Chem. C* **2009**, *113*, 5336.
(61) Liu, J. P.; Li, Y. Y.; Huang, X. T.; Ding, R. M.; Hu, Y. Y.; Jiang, J.; Liao, L. *J. Mater. Chem.* **2009**, *19*, 1859.

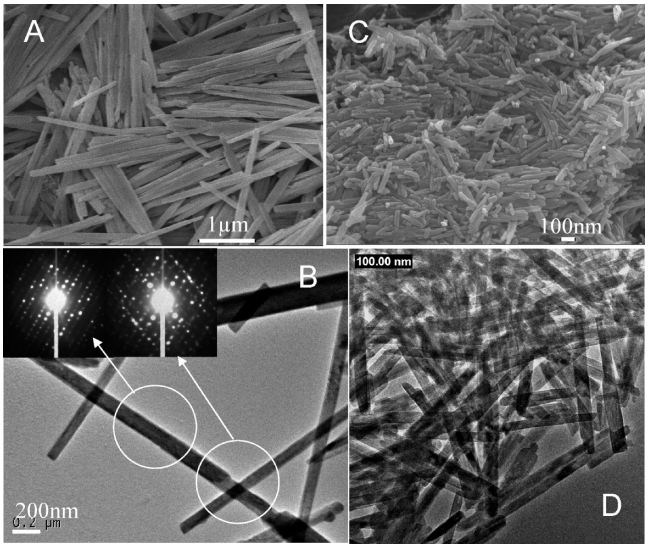

Figure 4. FESEM image (A) and TEM image (B) of $CoMoO_4 \cdot nH_2O$ sample prepared at 200 °C, 6 h, $r = 0$; (C) and (D) are FESEM and TEM images of $CoMoO_4 \cdot nH_2O$ sample prepared at 180 °C, 12 h, with $r = 1$.

grown on Au substrates. In general, these supported films are quite stable and can sustain vigorous stirring in solution, which indicates good adhesion with the substrate. The electrochemical, magnetic, and optical properties of these unique self-supported nanowire arrays will be studied. This facile self-assembly route to prepare self-supported nanowire arrays grown directly on a substrate might be general and extendable to other metal molybdates and tungstates.

It is apparent that ethanol plays an important role in controlling the size of as-prepared nanorods in terms of both length and diameter. The effect of other alcohols has also been investigated. It appears that methanol does not have an obvious effect on size, while the effect of isopropanol is similar to that of ethanol. Since ethanol is not included in the final product as confirmed by FTIR spectra (Figure 2), it is suggested that ethanol functions through altering the polar properties of the synthesis solution although the true mechanism remains unknown.[62] A set of experiments was conducted with different volumetric ethanol/water ratios (r = 0−2) to investigate the effect of the r value on morphology. The results show that an r value of 1 and below generally produces a mixture of nanorods and irregular particles, and with $r = 2$, almost 100% yield of the nanorods can be achieved. However, the effect on size of nanorods is no longer pronounced for r = 1−2. A similar synthetic strategy can also be applied to the preparation of $CoMoO_4 \cdot nH_2O$ nanorods. Figure 4 shows the as-prepared $CoMoO_4 \cdot nH_2O$ nanorods with or without addition of ethanol. The nanorods (Figure 4A,B) prepared without ethanol also usually form bundles with diameters of 100−200 nm and lengths up to 10 μm. The appropriate temperature for synthesis of $CoMoO_4 \cdot nH_2O$ nanorods was generalized to 180−200 °C. With ethanol, as shown in Figure 4C,D, the monodispersed $CoMoO_4 \cdot nH_2O$

(62) Chang, Y.; Zeng, H. C. *Cryst. Growth Design* **2004**, *4*, 273.

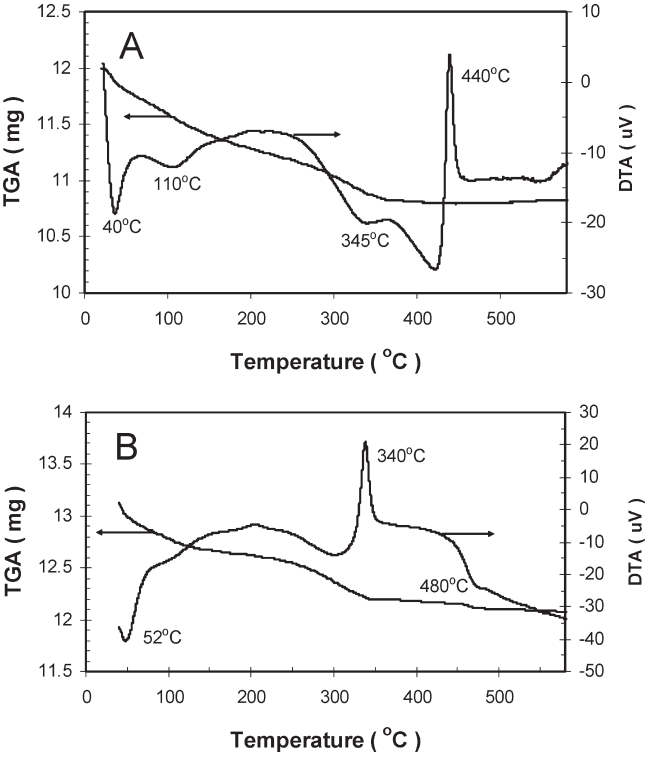

Figure 5. Typical TG-DTA curves for $NiMoO_4 \cdot nH_2O$ sample (A) and $CoMoO_4 \cdot nH_2O$ sample (B).

nanorods are generally straight and smooth and have a constant diameter (20−30 nm) along the growth direction. The ED patterns in Figures 3C and 4B clearly show that the as-prepared nanorods are single-crystalline.

The dehydration process is investigated utilizing the TG-DTA technique as shown in Figure 5. From Figure 5A (a typical TGA curve for $NiMoO_4 \cdot nH_2O$), the weight becomes stable below 400 °C, which is rather different from reported dehydration process for this hydrate compound prepared by other routes although one also observes three main stages of weight loss.[29,33] The desorption below 100 °C which corresponds to an endothermic peak on the DTA curve is generally attributed to the evolution of reversibly bound water molecules. The desorption above 100 °C up to 300 °C may be associated with evolution of water molecules that form an integral part of the crystal structure of $NiMoO_4 \cdot nH_2O$.[29,33] The weight loss between 300 and 400 °C which corresponds to a broad endothermic peak on the DTA curve is attributed to the evolution of water molecules reversibly bound to the hydrate crystal phase instead of β-isomorph since at this temperature phase transformation has not yet taken place as will be discussed shortly. The TGA curve (Figure 5B) of $CoMoO_4 \cdot nH_2O$ is similar to that of $NiMoO_4 \cdot nH_2O$ but with an additional weight loss step around 350−470 °C. This desorption feature may be attributed to the evolution of water molecules from the β-isomorph for the reason that in this temperature range, the hydrate crystal structure has transformed to the β phase. For both $NiMoO_4 \cdot nH_2O$ and $CoMoO_4 \cdot nH_2O$, the overall percentage weight loss varies sample by sample but generally is in the range of 7.5−9.1%,

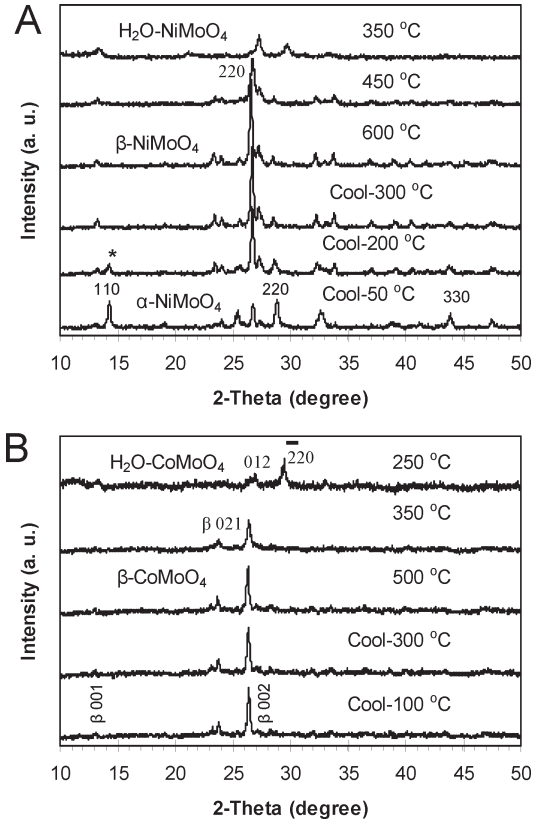

Figure 6. (A) Time-resolved XRD powder diffraction patterns for $NiMoO_4 \cdot nH_2O$ (150 °C, 6 h, $r = 0$) as a function of temperature. Cool-temp represents the sample is cooled down to this temp after being heated to 600 °C. (B) Time-resolved XRD powder diffraction patterns for $CoMoO_4 \cdot nH_2O$ (180 °C, 8 h, $r = 0$) as a function of temperature. Cool-temp represents the sample is cooled down to this temp after being heated to 500 °C.

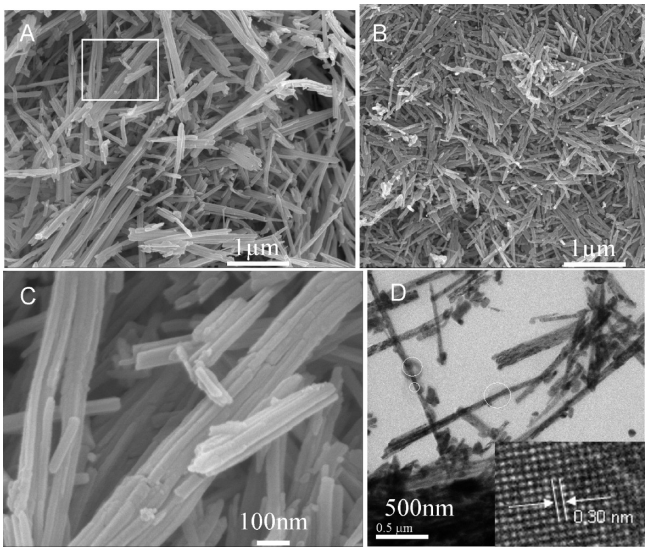

Figure 7. Product obtained by annealing $NiMoO_4 \cdot nH_2O$ at 450 °C for 1 h with a ramp of 1 °C min^{-1}: (A) prepared at 150 °C, 6 h, and $r = 0$; (B) prepared at 150 °C, 6 h, and $r = 2$; (C) high-magnification FESEM image corresponding to indicated area in (a). (D) TEM image of product obtained by annealing $NiMoO_4 \cdot nH_2O$ (150 °C, 6 h, and $r = 0$) at 600 °C for 1 h with a ramp of 5 °C min^{-1}, inset is a lattice-resolved TEM image showing a lattice constant of 0.30 nm.

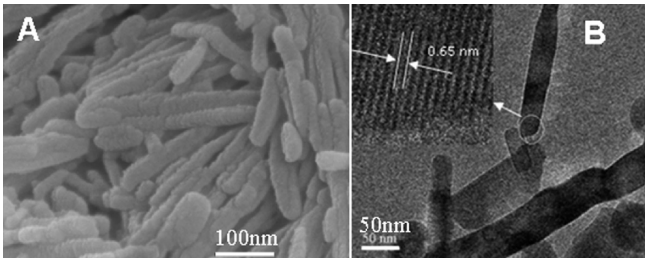

Figure 8. (A) FESEM image of β-$CoMoO_4$ nanorods by annealing $CoMoO_4 \cdot nH_2O$ (prepared at 180 °C, 12 h, $r = 1$) at 350 °C for 1 h with a ramp of 1 °C min^{-1}; (B) TEM image of $CoMoO_4$ nanorods after annealing $CoMoO_4 \cdot nH_2O$ (prepared at 180 °C, 12 h, $r = 1$) at 600 °C for 1 h, inset is a lattice-resolved TEM image taken on selected area indicated with an unfilled white circle showing a interlayer spacing of 0.65 nm.

corresponding to an n value of 0.99−1.22. Analysis based on nine samples (six Ni−Mo, three Co−Mo) gives an average n value of 1.11.

The most notable characteristics of the DTA curves are the strong exothermic peaks. This peak centers at 440 and 340 °C for $NiMoO_4 \cdot nH_2O$ and $CoMoO_4 \cdot nH_2O$, respectively. These peaks correspond to crystal phase transformation from the hydrate phase directly to the β phase possibly because of their crystal structural similarity.[29,33] However, it must be noted that the transformation temperatures are significantly higher than reported values. One previous study reported that the transformation from the hydrate phase to the β phase takes place rapidly at temperatures of 320 and 240 °C for $NiMoO_4 \cdot nH_2O$ and $CoMoO_4 \cdot nH_2O$,[29,33] respectively. One may attribute this difference to different preparation methods which lead to different size and shape of materials.

To better visualize the complex phase transformation processes, time-resolved synchrotron XRD is employed. Figure 6A displays a series of XRD patterns for a $NiMoO_4 \cdot nH_2O$ sample as a function of temperature. As can be seen, the pattern taken at 350 °C is identical with the room temperature pattern of $NiMoO_4 \cdot nH_2O$ (Figure 1A), which indicates that the phase transition has not started. From differential thermal analysis (DTA) above, the phase transformation temperature is around 440 °C for $NiMoO_4 \cdot nH_2O$ (JCPDS card no. 13-0128). This is indeed verified as the pattern taken at 450 °C no longer remains the same but can be indexed to β-$NiMoO_4$ isomorph (JCPDS card no. 12-0348) as indicated by the appearance of the characteristic (220) peak at 26.6°. Further heating the sample up to 600 °C does not produce any phase transition since the β-$NiMoO_4$ is stable up to 730 °C.[29,33] After reaching 600 °C, the sample was cooled down. When the sample was cooled down to 200 °C, a new set of peaks in the XRD pattern start to appear indicating onset of phase transition, which can be clearly seen with the emerging of a new peak at around 14.3° (marked with an asterisk in Figure 6A). This peak is in fact originated from the (110) diffraction of α-$NiMoO_4$ phase, and the increase in intensity of this peak means a growing amount of the α-$NiMoO_4$ phase in the sample. Further cooling the sample to 50 °C produces a pure α-$NiMoO_4$ isomorph since the XRD pattern can be perfectly indexed to α-$NiMoO_4$ (JCPDS card no.

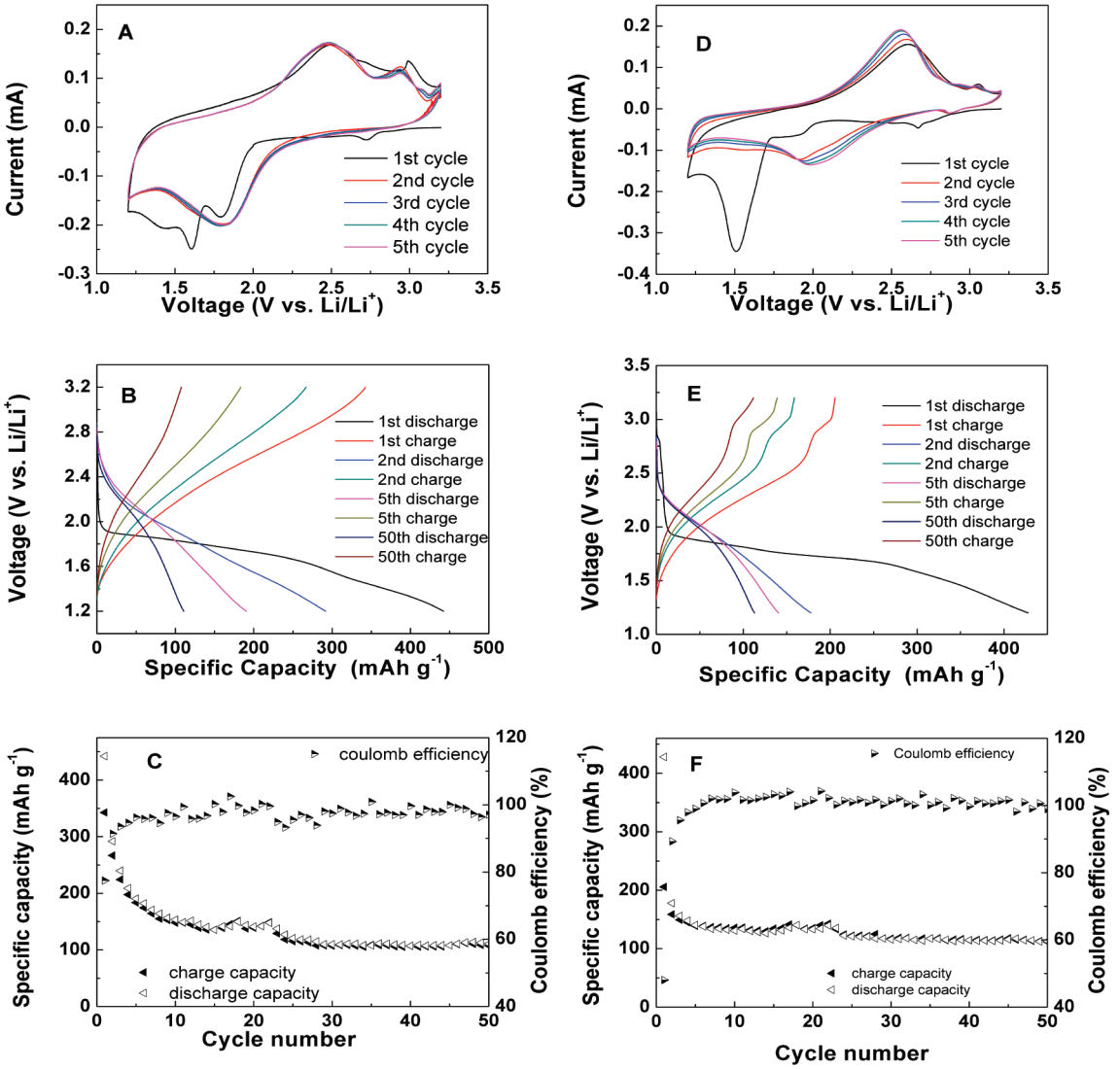

Figure 9. Cyclic voltammograms with a scan rate of 0.5 mV s^{-1} for the first five cycles, voltage-capacity profiles with a current density of 50 mA g^{-1}, and cycling performances of $NiMoO_4$ (A, B, and C) and $CoMoO_4$ (D, E, and F) nanorod electrodes between 1.2 and 3.2 V (vs Li^+/Li). $NiMoO_4$ nanorod was obtained by annealing the $NiMoO_4 \cdot nH_2O$ sample (150 °C, 6 h, $r = 0$) at 400 °C for 1 h. $CoMoO_4$ nanorod was obtained by annealing the $CoMoO_4 \cdot nH_2O$ sample (180 °C, 12 h, $r = 0$) at 300 °C for 1 h.

33-0948).[29,33,36] This is expected noting that β-$NiMoO_4$ cannot be quenched to room temperature. FTIR (Figure 2A, c and d) spectra are also taken on calcined samples, which further confirm the formation of α-$NiMoO_4$ by comparing with reported spectra.[36] Overall, the process can be expressed as $NiMoO_4 \cdot nH_2O \rightarrow \beta$-$NiMoO_4 \rightarrow$ α-$NiMoO_4$. For the Co−Mo system, the phase transformation process appears more complicated because β-$CoMoO_4$ can be quenched to room temperature. Therefore, the product after annealing could be a mixture of α-$CoMoO_4$ and β-$CoMoO_4$ although the pure β-$CoMoO_4$ phase can be obtained using a high cooling rate. Figure 6B gives a set of XRD patterns as a function of temperature. In agreement with the DTA analysis, $CoMoO_4 \cdot nH_2O$ does not transform to β-$CoMoO_4$ until around 350 °C. The pattern taken at 350 °C can be satisfactorily indexed to β-$CoMoO_4$ (JCPDS card no. 21-0868).[29,33,36] Further heating up to 500 °C and cooling down to 100 °C do not produce any alteration in XRD patterns. This means that the α-$CoMoO_4$ isomorph was not formed in our XRD experiment. The FTIR spectra (Figure 2B, c and d) of calcined samples in general agree well with reported spectra of β-$CoMoO_4$ although grinding β-$CoMoO_4$ with KBr may result in partial transformation to α-$CoMoO_4$.[36]

The morphology of calcined samples is also examined with FESEM/HRTEM. Figure 7 displays as-obtained α-$NiMoO_4$ nanorods after annealing at either 450 or 600 °C. Clearly, the nanorod morphology is largely retained. It is interesting to note that some rods become curved (Figure 7A), which may be explained by considering the thermally induced strain. Also because of the strain, the original small filaments closely assembled in a bundle start to peel away from each other resulting in some broken short nanorods (Figure 7C). Note that at 450 °C which is just around the phase transition temperature, decomposition and crystallization take place largely in small domains. TEM observation (Figure 7D) reveals a porous (nonsmooth) structure made up of fine nanoparticles, which is reconfirmed by BET surface area

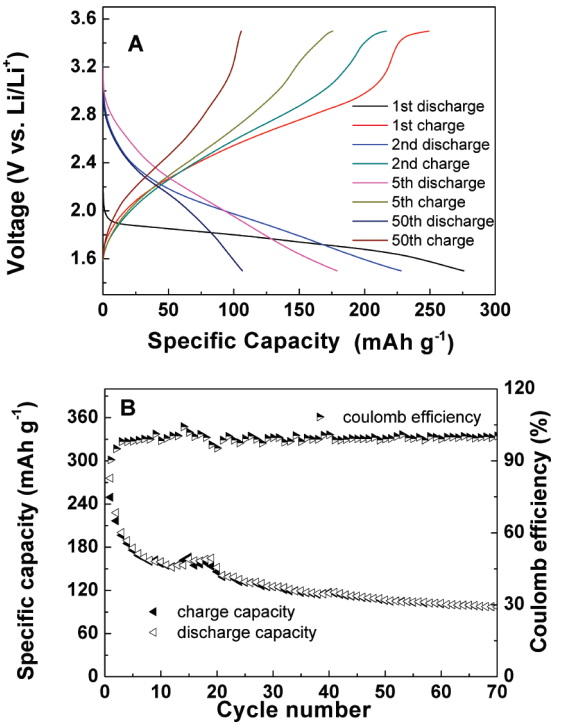

Figure 10. Voltage−capacity profiles (A) and cycle performances (B) of $NiMoO_4$ nanorod electrodes between 1.5 and 3.5 V (vs Li^+/Li) with a current density is 50 mA g^{-1}. $NiMoO_4$ nanorod was obtained by annealing the $NiMoO_4 \cdot nH_2O$ sample (150 °C, 6 h, $r = 0$) at 400 °C for 1 h. $CoMoO_4$ nanorod was obtained by annealing the $CoMoO_4 \cdot nH_2O$ sample (180 °C, 12 h, $r = 0$) at 300 °C for 1 h.

measurement shortly. When the sample is heated to 600 °C with a ramp of 5 °C min^{-1}, the product becomes better crystallized (Figure 7D and inset). Annealing smaller nanorods (prepared with addition of ethanol) at 450 °C leads to necklace-like 1D nanostructures (Figure 7B). However, if annealed at 600 °C, most nanorod bundles fuse together to form either larger nanorods or particles (not shown here). Similarly, β-$CoMoO_4$ nanorods can be obtained by annealing hydrate precursor at 350 °C as shown in Figure 8A. Clearly, the nanorod morphology is essentially unaltered after thermal treatment at a relatively low temperature (350 °C) in comparison with Figure 4C. When annealed at 600 °C, a large number of smaller nanorods transform into elongated platelets (Figure 8B) with high crystallinity (Figure 8B, inset). However, for large rods synthesized without adding ethanol (Figure 4A), no obvious morphology alteration is observed even annealed at 600 °C.

Considering that the as-synthesized $AMoO_4$ nanorods may find application in catalysis, electrode material, and sensors, as an example, we measured the surface area of $NiMoO_4$ nanorods (annealed at 450 °C, Figure 7A) using the Brunauer−Emmett−Teller (BET) technique carried out at the liquid nitrogen temperature. The surface area calculated using the multipoint BET method is found to be 65 m^2 g^{-1}. This is relatively large compared to a reported value of 29 m^2 g^{-1},[28] which is consistent with the TEM observation of a porous (nonsmooth) structure (Figure 7D).

The lithium storage capability of AMO_4 (A = Ni, Co) nanorods is investigated by cyclic voltammetry (CV) and charge/discharge cycling. $NiMoO_4$ nanorods are obtained by annealing the $NiMoO_4 \cdot nH_2O$ sample (150 °C, 6 h, $r = 0$) at 400 °C for 1 h. $CoMoO_4$ nanorods are obtained by annealing the $CoMoO_4 \cdot nH_2O$ sample (180 °C, 12 h, $r = 0$) at 300 °C for 1 h. On the basis of the above TGA, XRD, and SEM characterizations, the employed annealing temperatures are high enough for elimination of both physically and chemically absorbed hydrates but without causing phase transformations and destruction of the nanorod microstructures. Figure 9 shows the electrochemical performance of $AMoO_4$ (A = Ni, Co) nanorods between 1.2 and 3.2 V (vs Li^+/Li). Apparently, both molybdates manifest similar charge/discharge processes based on the CVs and the voltage−capacity profiles. Unlike the reversible lithium intercalation/deintercalation mechanism for MoO_3 with a layered crystal structure,[63] there exist clearly different electrochemical properties between the first cycle and the subsequent cycles for $AMoO_4$ (A = Ni, Co) nanorods. Though the detailed mechanism of the charge/discharge processes in $AMoO_4$ (A = Ni, Co) nanorods can be extremely complicated and remains unknown, the charge/discharge processes in $AMoO_4$ (A = Ni, Co) nanorods might be inferred on the basis of the results shown in Figure 9 and reported results on other molybdates.[51−53] Specifically, the first discharge is essentially a crystal structure destruction process which yields a mixture of an inert matrix, Li−A−O, and an electrochemical active Li_xMoO_y phase.[51] The formation of Li−A−O is irreversible and contributes to the irreversible capacity loss in the first cycle. Additionally, the formation of a solid electrolyte interface (SEI) layer is also partly responsible for the initial irreversible capacity loss. In the following charge/discharge cycles, the electrochemically active Li_xMoO_y conveys reversible electrochemical reactivity toward Li. The highly reversible formation/decomposition of the Li_xMoO_y phase results in a nearly 100% Coulomb efficiency in the following cycles. The specific capacity of $AMoO_4$ nanorods fades off quickly in the course of the first five cycles and then becomes stable subsequently. The initial rapid fading may be due to large specific volume changes and loss of electric contacts. Despite the initial fading, capacities of about 120 mA h g^{-1} can be retained after 50 cycles (Figure 9 C,F). To the best of our knowledge, most reports on the lithium reactivity of molybdates are focused on their potential application as anode materials for LIBs.[51−53] In fact, from the results above, $AMoO_4$ nanorods manifest reversible lithium reactivity at potentials more positive than 1.5 V, which may suggest their possible use as safer cathode materials in future LIBs. This hypothesis is further supported by the charge/discharge cycling performance of $NiMoO_4$ nanorods at potentials between 1.5 and 3.5 V as shown in Figure 10. The $NiMoO_4$ nanorods manifest specific

(63) Li, W. Y.; Cheng, F. Y.; Tao, Z. L.; Chen, J. *J. Phys. Chem. B* **2006**, *110*, 119.

discharge capacities of 275, 230, and 180 mA h g^{-1} for the first, second, and fifth cycle, respectively. Even after 70 cycles, a capacity of 100 mA h g^{-1} can still be retained. The above preliminary results imply that nanostructured molybdates might be used as cathode materials for future LIBs. Research in this area is currently undertaken in this group.

4. Conclusions

In summary, nanorods of $NiMoO_4 \cdot nH_2O$ (with diameter of 50−100 nm and length up to 10 μm) and $CoMoO_4 \cdot nH_2O$ (with diameter of 100−200 nm and length up to 10 μm) can be synthesized by a facile hydrothermal method. The appropriate temperatures for synthesis of $NiMoO_4 \cdot nH_2O$ and $CoMoO_4 \cdot nH_2O$ nanorods are found to be 150 and 180 °C, respectively. The size of the nanorods can be simply controlled by adding ethanol in the synthesis solution, leading to smaller nanorods with diameters around 20−30 nm and up to 1 μm in length. Importantly, the self-assembled growth of aligned $NiMoO_4 \cdot nH_2O$ nanorod arrays on Ti-foil substrates is also achieved. $AMoO_4 \cdot nH_2O$ (A = Ni, Co) nanorods synthesized in present study are found to be more thermally stable by over 100 °C compared to that reported in previous studies. The onset temperatures for phase transformation are around 440 and 340 °C for $NiMoO_4 \cdot nH_2O$ and $CoMoO_4 \cdot nH_2O$, respectively. After thermal dehydration and phase transformation, the 1D morphology can be largely retained. The dehydrated $AMoO_4$ nanorods can be used for reversible lithium storage. As an example, when cycled in the voltage window of 1.5−3.5 V, $NiMoO_4$ nanorods manifest a reversible capacity of 100 mA h g^{-1} after 70 cycles.

Acknowledgment. The authors are grateful to Prof. Hua Chun Zeng (department of chemical and biomolecular engineering, National University of Singapore) for allowing use of his facilities and to Nanyang Technological University for financial support through the start-up grant (SUG).